ScienceDirect

International Journal of Hydrogen Energy
Volume 47, Issue 67, 5 August 2022, Pages 28956-28968

Numerical modelling of H_2 storage with cushion gas of CO_2 in subsurface porous media: Filter effects of CO_2 solubility

G. Wang, G. Pickup, K. Sorbie, E. Mackay

Show more

Outline | Share | Cite

https://doi.org/10.1016/j.ijhydene.2022.06.201

Highlights

- An extra 30% volume of CO_2 is required when considering CO_2 solubility.
- Back produced H_2 purity depends strongly on the hydrodynamics of H_2 and CO_2.
- "Filter" effects due to CO_2 solubility are identified for the first time.
- CO_2–H_2 mixing zone is expanded due to CO_2 solubility in gravity-stable regimes.

- Best H_2 recovery performance occurs in the gravity-dominated scenario.

Abstract

The central objective of this study is to improve the understanding of flow behaviour during hydrogen (H_2) storage in subsurface porous media, with a cushion gas of carbon dioxide (CO_2). In this study, we investigate the interactions between various factors driving the flow behaviour, including the underlying permeability heterogeneity, viscous instability, and the balance between the viscous and gravity forces. In particular, we study the impact of CO_2 solubility in water on the level of H_2 purity. This effect is demonstrated for the first time in the context of H_2 storage. We have performed a range of 2D vertical cross-sectional simulations at the decametre scale with a very fine cell size (0.1 m) to capture the flow behaviour in detail. This is done since it is at this scale that much of the mixing between injected and native fluids occurs in physical porous media. It is found that CO_2 solubility may have different (positive and negative) impacts on the H_2 recovery performance (i.e., on the purity of the produced H_2), depending on the flow regimes in the system. In the viscous dominated regime, the less viscous H_2 may infiltrate and bypass the cushion gas of CO_2 during the period of H_2 injection. This leads to a quick and dramatic reduction in the H_2 purity when back producing H_2 due to the co-production of the previously bypassed CO_2. Interestingly, the impurity levels in the H_2 are much less severe in the case when CO_2 solubility in water is considered. This is because the bypassed CO_2 will redissolve into the water surrounding the bypassed zones, which greatly retards the movement of CO_2 towards the producer. In the gravity dominated scenario, H_2 accumulates at the top of the model and displaces the underlying cushion gas in an almost piston-like fashion. Approximately 58% of H_2 can be recovered at a purity level above 98% (combustion requirements by ISO) in this gravity-dominated case. However, when CO_2 solubility is considered, the H_2 recovery performance is slightly degraded. This is because the dissolved CO_2 is also gradually vaporised during H_2 injection, which leads to an expansion of mixing zone of CO_2 and H_2. This in turn reduces the period of high H_2 purity level (>98%) during back-production.

Previous Next

Keywords

Underground hydrogen storage; H_2 purity; CO_2 solubility; CO_2 cushion gas; Fine-scale flow simulation

Introduction

The target of "Net Zero" has been set out to limit the increase in global temperature below 1.5 °C compared with the pre-industrial level [1]. The term "Net Zero" means completely negating the amount of greenhouse gases produced by human activities to mitigate climate change [2,3]. Clearly, this goal fundamentally relies on the energy transition from fossil fuels to renewable energy technologies such as solar and wind energy [4].

Currently, the application of renewable energy technology is restricted by their nature of intermittency and uncertainty, which puts energy security and reliability at risk [5]. Therefore, appropriate energy storage technologies must be developed to progress the deployment of renewable energies. One of the viable solutions is the use of hydrogen (H_2) as an energy storage vector [6,7]. H_2 has very high energy density (33.3 kWh/kg) and produces only water when combusted [8,9]. The electricity produced from renewable energies can be used to split water to H_2 (and oxygen) via electrolysis, i.e., the concept "power-to-gas" [10]. As a clean fuel, H_2 is then combusted to provide energy/heat when the demand increases [11,12]. Such flexibility can secure the energy supply and unlock the potential of renewable energies. However, the success of this process requires large storage capacity for the significant amounts of H_2 involved at grid scale [13,14]. This is because H_2 has a very low mass density and is difficult to compress and liquefy [15].

Underground gas storage (UGS), which potentially has tremendous storage capacity, is increasingly considered as a necessary part of the supply chain for H_2 energy [16,17]. Typical subsurface storage can be categorized into 3 types: salt caverns, depleted hydrocarbon reservoirs and saline aquifers. In fact, H_2 storage in salt caverns has been successfully applied in the past, primarily for use in oil refining and ammonia production [18]. Due to the advantage of high operational efficiency, some researchers proposed to progress H_2 storage in salt caverns for energy transition [19,20]. However, this option is subject to the sufficient thickness of salt deposits and therefore its availability is much limited [[21], [22], [23]]. On the other hand, saline aquifers and depleted gas reservoirs, which have wider availabilities and larger storage capacities, are considered more suitable for decarbonizing the energy sector at scale [24]. In this research, our study is based on a synthetic aquifer. We will test the feasibility of H_2 storage in depleted reservoirs in future work.

Gas storage in subsurface geological formations is not a new technology in the energy industry [25,26]. Cyclic injections and withdrawals of natural gas (working gas) were widely applied to smooth gas supplies to meet daily/seasonal fluctuations of energy demand [27]. In addition to the working gas, a certain amount of cushion gas (usually the same as the working gas), may need to be injected in advance to provide pressure support for the back-production of working gas. This cushion gas is not extracted and remains in the subsurface formations. Unlike

natural gas storage, H_2 generation, such as via electrolysis, still requires very high capital and operation expenses [28,29]. Hence, a different type of cushion gas may be a more cost-effective operational strategy for H_2 storage [30]. For this reason, this study tests the idea of using CO_2 as cushion gas, which provides an extra benefit of directly reducing CO_2 emissions.

Recently, a range of techno-economic case studies were conducted to examine the feasibility of H_2 storage based on specific fields [[31], [32], [33]]. These field-scale studies identified the practical and economic factors determining the viability of H_2 storage. However, very limited studies can be found in literature focusing on fundamental understandings of the hydrodynamic flow behaviour of H_2 with CO_2 as cushion gas in the subsurface porous media. Much work remains to be done to identify and understand the key factors influencing the migration and distribution of fluids [34,35].

The flow behaviour in subsurface porous media is controlled by the interactions between the fluid characteristics, medium properties and various driving forces [36]. Depending on the relative contributions of these factors, the flow regimes can be categorized according to scaling theory [[37], [38], [39]]. For example, in viscous-dominated flow the displacement process is dominantly controlled by the viscous instability whereas in the gravity-dominated regime, strong gravity segregation may be observed [40].

In a previous study [41], the key flowing features occurring in viscous-dominated to gravity-dominated scenarios have been systematically demonstrated in the context of H_2 storage. Scaling theory was applied to assess the various flow regimes in terms of the force balances (viscous/gravity mainly) in systems of different sizes. The effects of the flow regimes and the related hydrodynamics on the final purity of the back produced H_2 was studied. In this paper, we extend this earlier work by determining the impact of CO_2 solubility on the purity of the produced H_2 from the storage reservoir. CO_2 solubility is in fact one of the key trapping mechanisms for underground CO_2 storage [[42], [43], [44]]. We demonstrate how the interactions between mechanisms of CO_2 dissolution, reservoir heterogeneity and multiphase flow behaviour, affect the H_2 recovery performance at specific levels of impurity. A range of very fine scale simulations, which are essential and necessary to capture the fluid behaviour in detail, are conducted. We present two extreme scenarios, namely the viscous-dominated and gravity-dominated flow regimes, with an aim of providing insight to optimize the operation strategy to improve the H_2 recovery performance. The outcome of this study together with our previous work, should also be useful to determine the required experimental work for projects of H_2 storage. The complete dataset of this numerical study can be found at https://doi.org/10.17861/615bdf45-a92b-4ff4-8f9e-efa6608ed030.

Methodology

The central purpose of this study is to conduct a detailed sensitivity analysis to identify the significant factors driving the flow behaviour of H_2 (working gas) and CO_2 (cushion gas), and thus the recovery performance of the H_2 and its purity. To achieve this, we performed a series of

flow simulations in a 2D vertical system, using a fully compositional reservoir simulator- CMG/GEM [45]. The modelling methods are mostly inherited from our previous work [41]. All the simulation configurations can be found in the data repository with the link given above. Here, we only outline the main input to which we refer later in this article when explaining our results.

Fluid model

Table 1 lists the modelled fluid properties based on the Peng-Robinson Equation of State (EOS) under initial reservoir conditions. The molecular diffusion was neglected as this study is based on a highly heterogeneous system, where convective dispersion dominates the flows. Note that the CO_2 is injected at supercritical conditions, but is referred to as "gas" in this paper.

Table 1. Fluid modelling using PR-EOS under initial reservoir conditions.

Equation of State (EOS)	**Cubic PR-EOS [46] with data by Ref. [47]**	
Initial reservoir conditions	**T = 51.9 °C; P = 15,000 kPa**	
Fluid properties	Viscosity (cp)	Density (k,g/m^3)
Hydrogen (H_2)	0.008	7.9
Carbon dioxide (CO_2)	0.032	630
Water	0.5	1010

Synthetic geo-model

As shown in Fig. 1, a correlated random permeability field (i.e. CRF) was created using Petrel [48] to mimic reservoir heterogeneity. Other realizations with the fixed geostatistical setting were also tested, and they essentially have very similar reservoir response. Therefore, we select this model as a representative case to demonstrate the flow behaviour of H_2 and CO_2, driven by various factors including viscous instability, gravity force, CO_2 solubility etc.

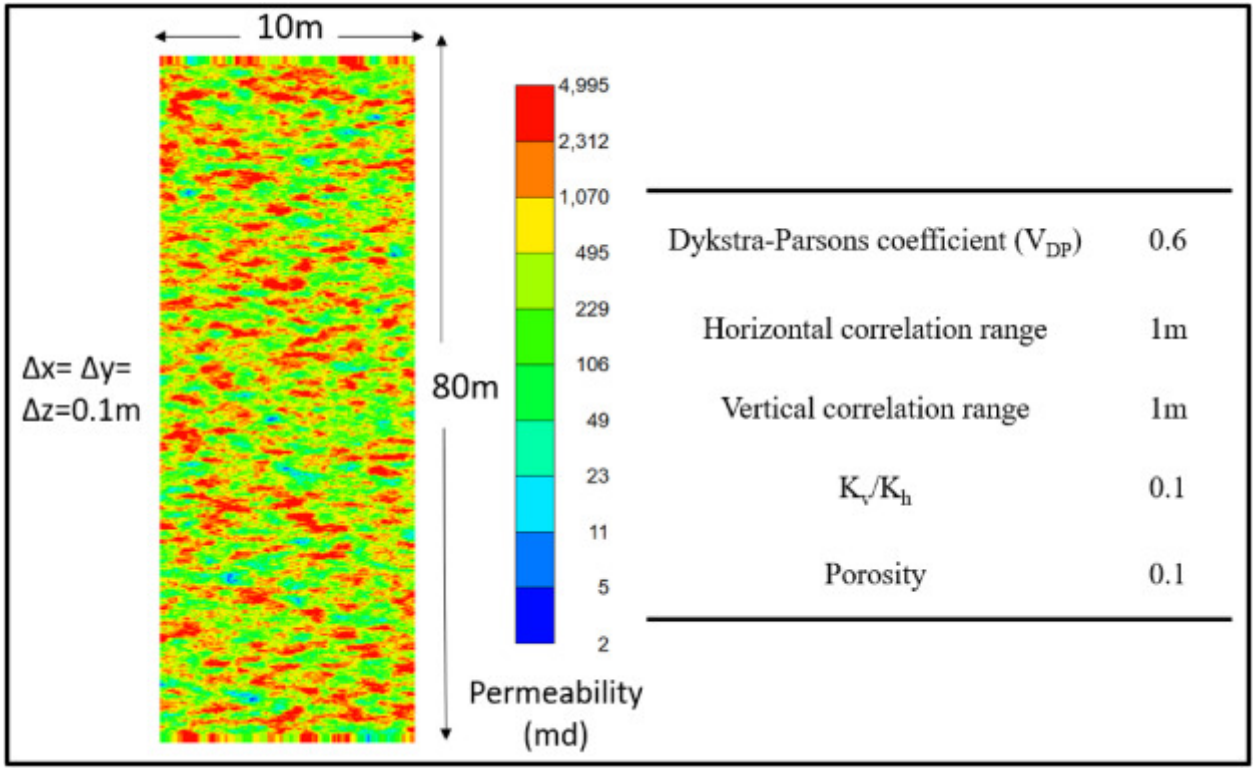

Download : Download high-res image (951KB) Download : Download full-size image

Fig. 1. The correlated heterogeneous permeability field used in this work.

Operation strategy

From our previous work [41], we have identified that the two key end member flow regimes encountered are, viscous-dominated and gravity-dominated flow regimes, although the flows can be in the transitional region where these forces are balanced. In this work, we extend that study to analyse how the CO_2 solubility influences the flow behaviour and thus the H_2 recovery in both scenarios; in particular, we focus on the issue of back produced H_2 purity. Operational strategies, which trigger the viscous-dominated and gravity-dominated flow regimes respectively, are outlined in Table 2 and Table 3. The operation rates in the viscous-dominated case are 100 times greater than that in the

gravity-dominated case. CO_2 is injected as a cushion gas first and then followed by the injection and production of H_2. The injected volume of CO_2 is twice as much by volume as H_2 under reservoir conditions. Both the injection and the production wells were horizontally perforated across the top and controlled by the flow rate at reservoir conditions. We assumed that the fracture pressure of the formation was never exceeded during the operation. The bottom of the model was set to mimic a large aquifer that allows fluid flow.

Viscous-dominated scenario:

Table 2. Operational strategy for viscous-dominated scenario.

Operational strategy	**0–1 day**	**1–1.5 days**	**1.5–2 days**
	CO_2 injection 0.15 pore volume/day	H_2 injection 0.15 pore volume/day	Back production 0.15 pore volume/day

Gravity-dominated scenario:

Table 3. Operational strategy for gravity-dominated scenario.

Operational strategy	**0–100 day**	**100–150 days**	**150–200 days**
	CO_2 injection 0.0015 pore volume/day	H_2 injection 0.0015 pore volume/day	Back production 0.0015 pore volume/day

Relative permeabilities and capillary pressure

In the system configured here, the period controlled by the two-phase flow mechanisms is primarily occurring at the displacing front, i.e., between CO_2 and water in our case. Fig. 2 shows the relative permeability curves for CO_2/brine, which are utilized here for modelling two-phase flow based on the experimental data produced by Ref. [49]. Capillary pressure is modelled using a synthetic Leverett J-function created in our previous work [41]. As the processes of gas injection and production involve strong flow reversals, the issue of gas trapping may arise and therefore is considered here. The Land constant (C) is set to 2.44 and this leads to a maximum trapped gas saturation (S_{grmax}) of 0.2 [50,51].

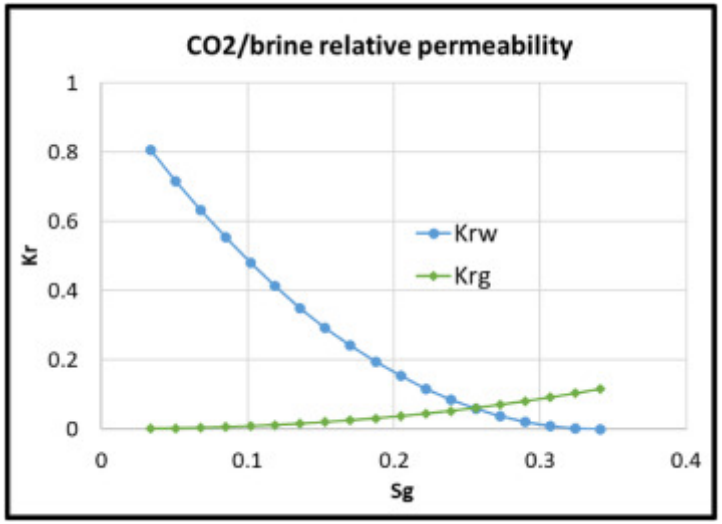

Download : Download high-res image (120KB) Download : Download full-size image

Fig. 2. Relative permeability curves for CO_2 (K_{rg}) and brine (K_{rw}), data by Ref. [49].

Solubility model

The solubility of gas in the aqueous phase is modelled based on Henry's Law (Equation (1)). The variation of Henry's law constant with respect to pressure and temperature is modelled by Equation (2) [[52], [53], [54]]. The effect of salinity is not included to simply the process. Note that the modelling method of Henry's law is assumed that the gaseous phase and the aqueous phase are in thermodynamic equilibrium. In practice, non-equilibrium CO_2 dissolution may occur, depending on the interface area between CO_2 and water and the operation timescale

[55]. The grid block residence times of the fluids are more than adequate for equilibrium to be established in the gravity-stable case, but there may be some deviation from equilibrium in the viscous dominated case. However, this is beyond the scope of this study and a detailed analysis of possible nonequilibrium effects may be required in the future.

Henry's law

$$f_{iw} = y_{iw} \cdot H_i \quad (1)$$

$$\ln H_i = \ln H_i^0 + V_i^\infty (p - p_i^0) / RT \quad (2)$$

where f_{iw} is the fugacity of the component i (CO_2 here) in the aqueous phase; y_{iw} denotes the mole fraction of component i in the aqueous phase; H_i is Henry's Law constant; H_i^0 is the reference Henry's Law constant; V^∞ is the partial molar volume of component i in the aqueous at infinite dilution [56]; P is its partial pressure in the gas phase under equilibrium conditions. P_i^0 is the reference pressure; R is gas constant; T is temperature. According to Ref. [57], $H^0{}_i$ is set to 3.3×10^{-4} mol/m$^3 \cdot$Pa at a reference temperature of 298.15 K under atmospheric pressure. We also compared our simulated results with the data in literature and the accuracy is acceptable, as shown in Fig. 3 [58].

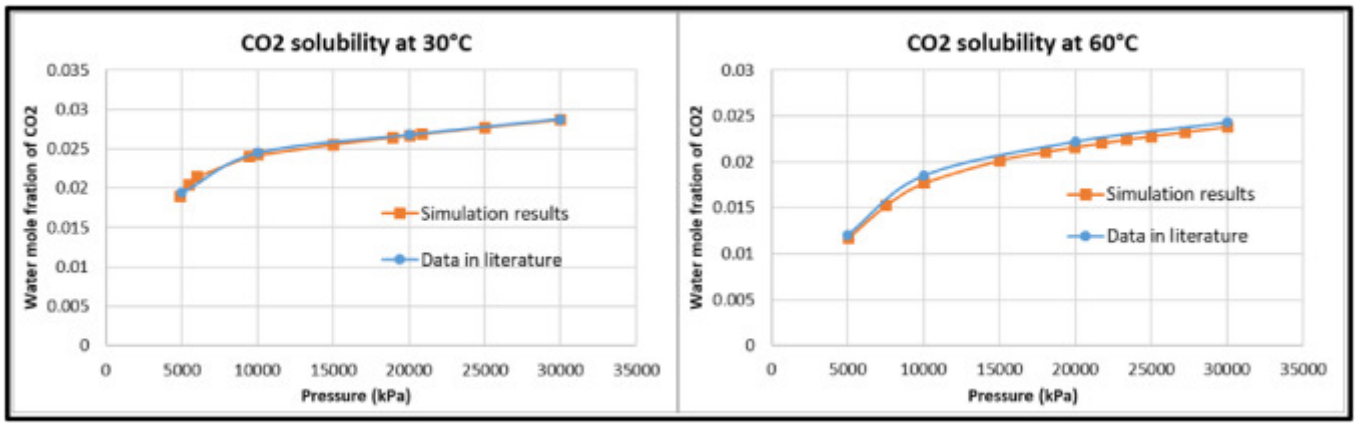

Download : Download high-res image (272KB) Download : Download full-size image

Fig. 3. Comparison between simulation results of CO_2 solubility with data by Ref. [58].

On the other hand, hydrogen solubility in water is much lower than CO_2 and therefore is ignored here [57]. In fact, we did conduct numerical tests with H_2 solubility activated, in which negligibly small changes in flow behaviour were observed. However, this does not exclude the necessity of taking H_2 solubility into account for H_2 storage in real systems. This is because even small amount of dissolved H_2 may potentially trigger biological and geo-chemical reactions, such as methanation and sulfur-reducing processes [59]. In a future publication, we will address how these reactions influence the recovery performance of H_2 and their potential impacts on the flow assurance.

Pseudo-tracer tests

A pseudo tracer analysis was conducted to uncover some of the flow mechanics due to CO_2 solubility in the viscous-dominated scenarios. These tests entail injecting a certain amount of CO_2 tracer, which had the exact same EOS data and solubility as CO_2. All the other simulation parameters were the same as the corresponding ones in previous regular simulations. The details of the tracer tests are outlined as below [60].

Injection location

The CO_2 tracer was injected into a grid block in one of the areas bypassed by H_2. These zones, which are occupied by CO_2 but bypassed by H_2, can be identified in the preliminary flow simulations.

Injection timing

To minimize the impacts of the tracer on the overall flow behaviour, the tracer injection was not conducted at the beginning of the simulation. Instead, the CO_2 tracer was injected slightly before the end of the H_2 injection, by which time the major bypassed zones have already formed.

Injection amount

A very small amount (almost negligible) of tracer was injected into the chosen bypassed grid block at a rate of 1.04e-8 PV/min for 15 min (1.56e-7 PV in total). We found that such a slow and small amount of injection has negligible impacts on the overall flow behaviour. However, the flow behaviour of the CO_2 tracer can be used to represent the actual flow trajectory of the CO_2 in bypassed areas during back production.

Results and discussion

A series of simulations were conducted and analysed to understand the impacts of CO_2 solubility on the flow behaviour. To clarify the purpose of each step of the analysis and the logic of this research, the results are presented in the following three steps (#1 to #3) outlined in Table 4. Note that the CO_2 solubility in water must lead to a reduction in the gas volume of CO_2 occupying in the pore space under reservoir conditions. To make the simulations with and without CO_2 solubility consistently comparable, the total amount of CO_2 injection in Cases with CO_2 solubility activated is increased to compensate for its dissolution in water. Due to the non-uniform gas distribution and pressure variations throughout the system, the total amount of the dissolved CO_2 cannot be determined a *priori* and therefore a series of trial-and-error tests was conducted. It turns out that an approximately 30% extra volume of CO_2 is required to achieve the same distance travelled by the gas displacing front at the end of gas injection. As seen in Fig. 4 and Fig. 10, the interface between gas and water (G/W) is indicated by two red arrows.

Table 4. Outline of numerical tests performed and objectives of each stage for this study.

Step	Flow scenarios	Objectives
#1	A. Viscous-dominated case B. Viscous-dominated case with CO_2 solubility	• To analyse the impacts of CO_2 solubility on H_2 recovery in the viscous-dominated flow regime
#2	C. Tracer test based on the Case A D. Tracer test based on the Case B	• To demonstrate the "filter effects" resulting from CO_2 solubility
#3	E. Gravity-dominated case F. Gravity-dominated case with CO_2 solubility	• To investigate the impacts of CO_2 solubility on H_2 recovery in the gravity-dominated flow regime

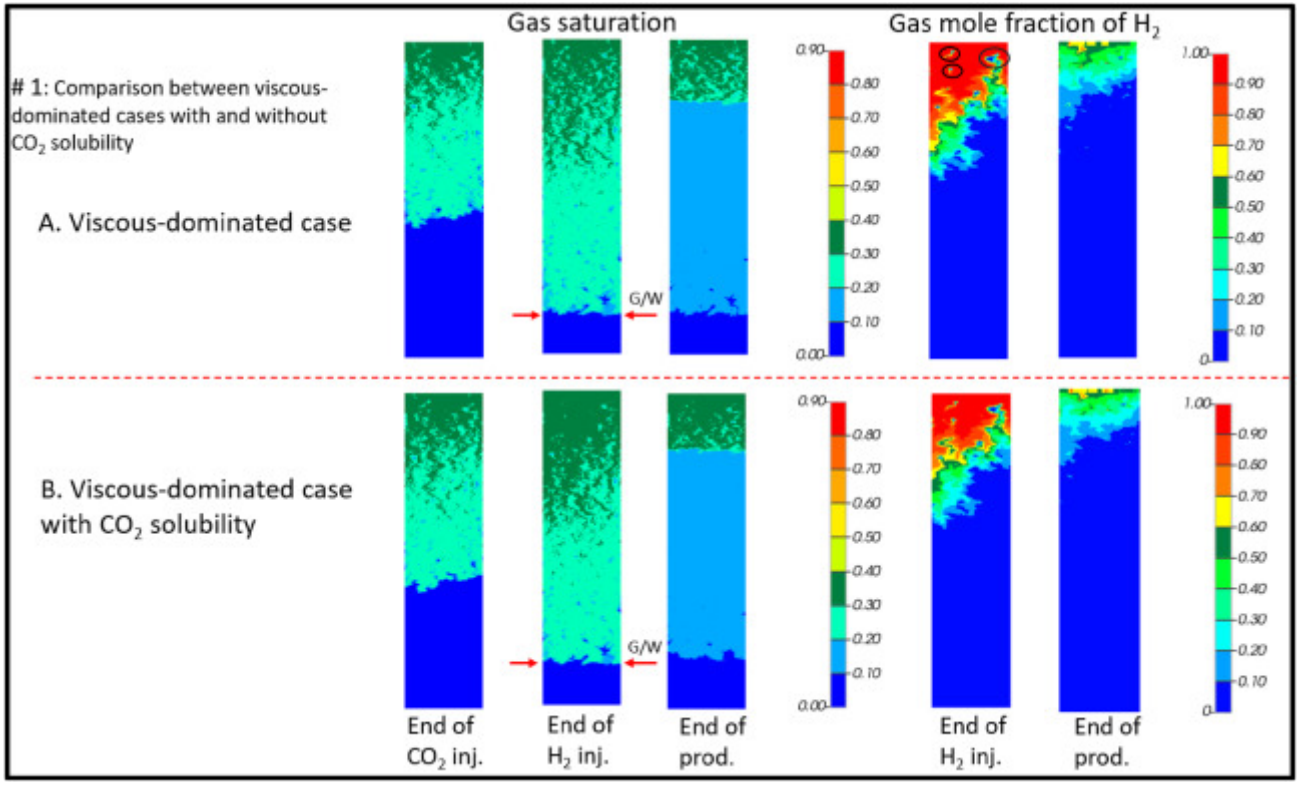

Download : Download high-res image (682KB) Download : Download full-size image

Fig. 4. Gas saturations and mole fractions of H_2 at the end of each cycle of the base model without CO_2 solubility (Case A at the top) and the case with CO_2 solubility (Case B at the bottom).

Impacts of CO_2 solubility in viscous-dominated flow scenarios

Results presented in this section are from the step #1 of the simulations listed in Table 4. In the injection sequence, there are two interfaces of interest, namely gas (CO_2)/water and CO_2/H_2, when investigating the hydrodynamic flow behaviour of H_2 and CO_2 in an aquifer. Fig. 4 is plotted to show the gas saturation (left side) and H_2 gas mole fraction (right side) of the viscous-dominated scenarios with/without CO_2

solubility activated. Within the system configured here, the gas displacing front is relatively stable without forming severe flowing fingers of gas in both cases (A&B). The reasons are twofold. The first is the poor gas relative permeability when the gas saturation is low, which self-stabilizes the interface between gas and water (see Fig. 2). The second is the correlation range (1 m × 1 m) of the permeability field is much lower than the system dimensions (10 m × 80 m) and therefore no dominant gas fingers into water arise [37,61]. In fact, the relatively stable interface between CO_2 and water guarantees no early water breakthrough during back production in the system configured here. This enables us to focus on the mixing zone between CO_2 and H_2, which is a potentially significant factor which may influence the H_2 purity during back production.

On the other hand, the interface between H_2 and CO_2, shows evident non-uniformity, as the mole fraction of H_2 is not evenly distributed above the CO_2 cushion gas (see the right part of Fig. 4). Within the underlying heterogenous permeability field, the less viscous H_2 does not proceed and displace the cushion gas of CO_2 in a piston-like fashion. It is not surprising that gas mixing occurs at the displacing front. More importantly, the cushion gas of CO_2 may be infiltrated and even **bypassed** by H_2 (indicated by the black ovals in Fig. 4A). Fig. 5 shows the H_2 purity in the back produced gas for Case A and B. Clearly, the bypassed CO_2 can be quickly co-produced, which leads to early reductions in H_2 purity during the back production. In particular, if certain high purity levels are required, then H_2 is poorly recovered. For example, the required purity levels of H_2 for fuel cell and combustion are 99.97% and 98%, respectively. From a practical perspective, the purification capacity of a processing terminal may vary significantly depending on the design of the processing system [62]. For example, a typical capacity of CO_2 purification based on ammonia (at an extra cost) of a processing terminal can manage up to 10% impurity of CO_2. Therefore, we tracked the H_2 recovery given the three critical threshold values of the H_2 purity mentioned above. As seen in Fig. 6, the H_2 recovery is only 9% (purity level >99.97%), 21% (purity level >98%) and 39% (purity level >90%) in Case A.

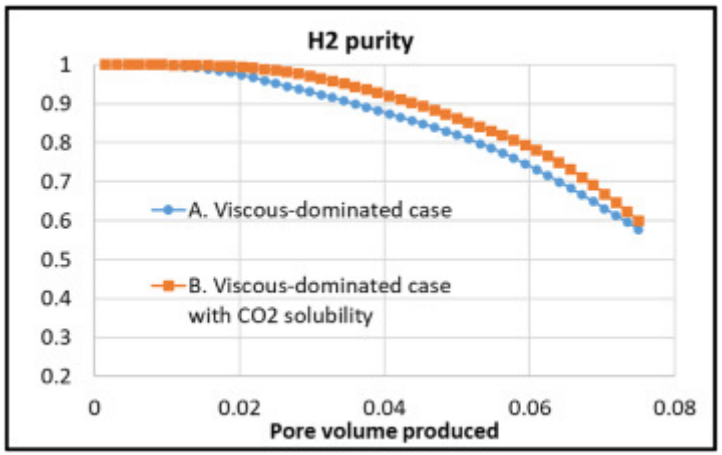

Fig. 5. The purity of back-produced H_2 of the viscous-dominated case (A) and the corresponding case with CO_2 solubility activated (B).

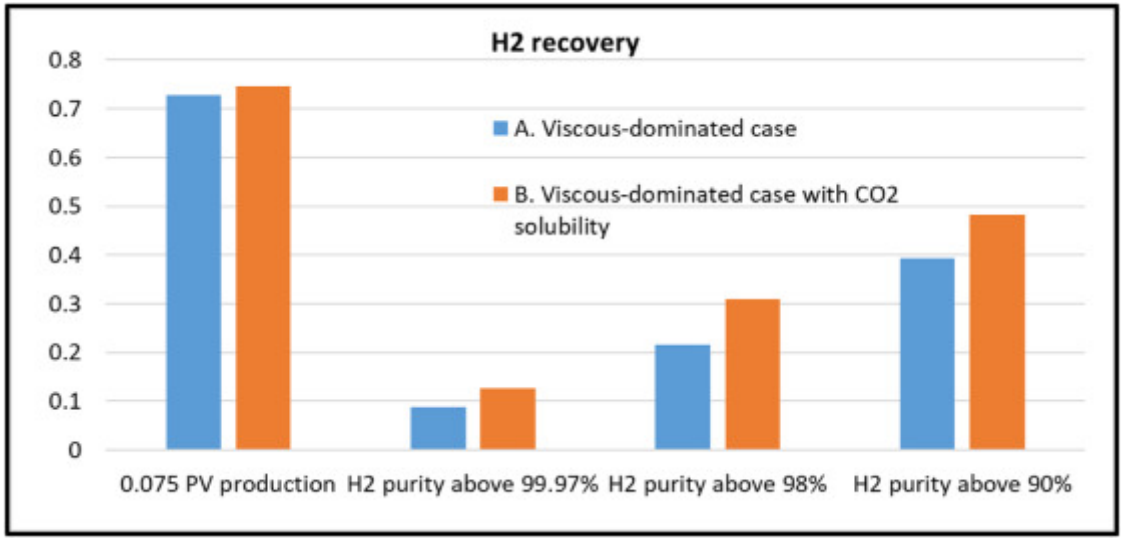

Fig. 6. Comparison of H_2 recovery between Case A&B at the end of 0.075 PV production, H_2 purity above 99.97%, 98% and 90%, respectively.

Surprisingly, although the flow behaviour of Case B (with CO_2 solubility) looks remarkably similar to Case A (see Fig. 4), the H_2 purity level during back production is improved when CO_2 solubility is included. The back produced H_2 purity profiles are compared for both cases in Fig. 5. As shown in Fig. 6, the H_2 recovery is increased by 2% at the end of production in Case B. More importantly, an extra of **4**%, **9.1** and **9.2**% of H_2 can be recovered, with a purity level above 99.97% (required for fuel cell) 98% (required for combustion) and 90% (typical processing capacity), respectively.

Tracer analysis

Clearly, the CO_2 solubility must lead to some flow mechanism that positively influences the H_2 recovery but cannot be easily observed from the snapshots of the gas saturations and component concentrations. To understand how the CO_2 solubility improves the H_2 recovery performance, we conducted a tracer analysis to track the flow trajectory of the CO_2 in the areas of flow bypassed during the H_2 injection phase. These are the step #2 simulations listed in Table 4.

As explained in the methodology section, we designed a tracer test, which entails injecting a tiny amount of tracer into a representative cell in the bypassed area. Fig. 7 (right side) is plotted to show the gas mole fraction of the CO_2 tracer at the end of injection. As seen in Fig. 7, we selected the one that is closest to the top producers. This is to ensure the impact of the bypassed CO_2 can be captured before the effects of the CO_2–H_2 mixing zone are observed at the production well. Otherwise, it is difficult to differentiate the impacts of the gas mixing (H_2 front) and the gas bypassing on the H_2 purity. The flow trajectory of the tracer is observed and compared between cases with and without including the CO_2 solubility in the simulations. Fig. 8 is plotted to compare the gas mole fraction of the tracer between two cases. As seen in Fig. 8, after the same pore volume of back-production (0.0063 PV), the tracer has reached the producer at the top in the case without CO_2 solubility (Case C) whereas the tracer distribution is much restricted in the case with CO_2 solubility (Case D). In other words, CO_2 solubility has retarded the breakthrough of the cushion gas (CO_2), which was bypassed during the period of H_2 injection.

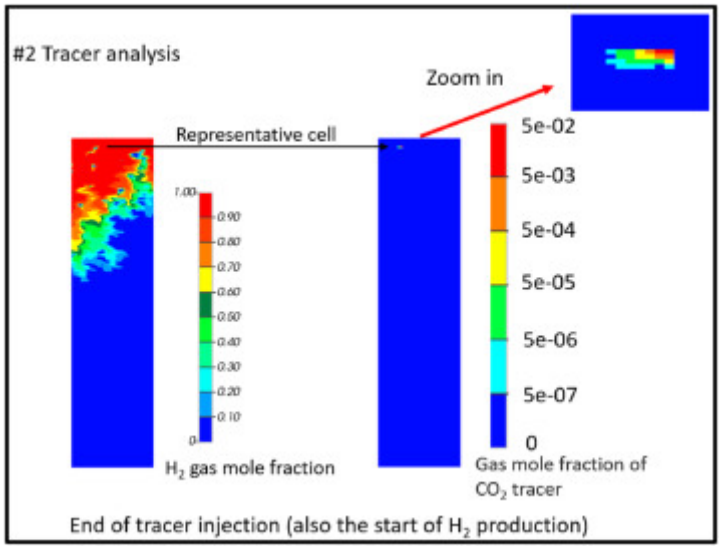

Download : Download high-res image (170KB) Download : Download full-size image

Fig. 7. Snapshot of tracer distribution at the end of tracer injection.

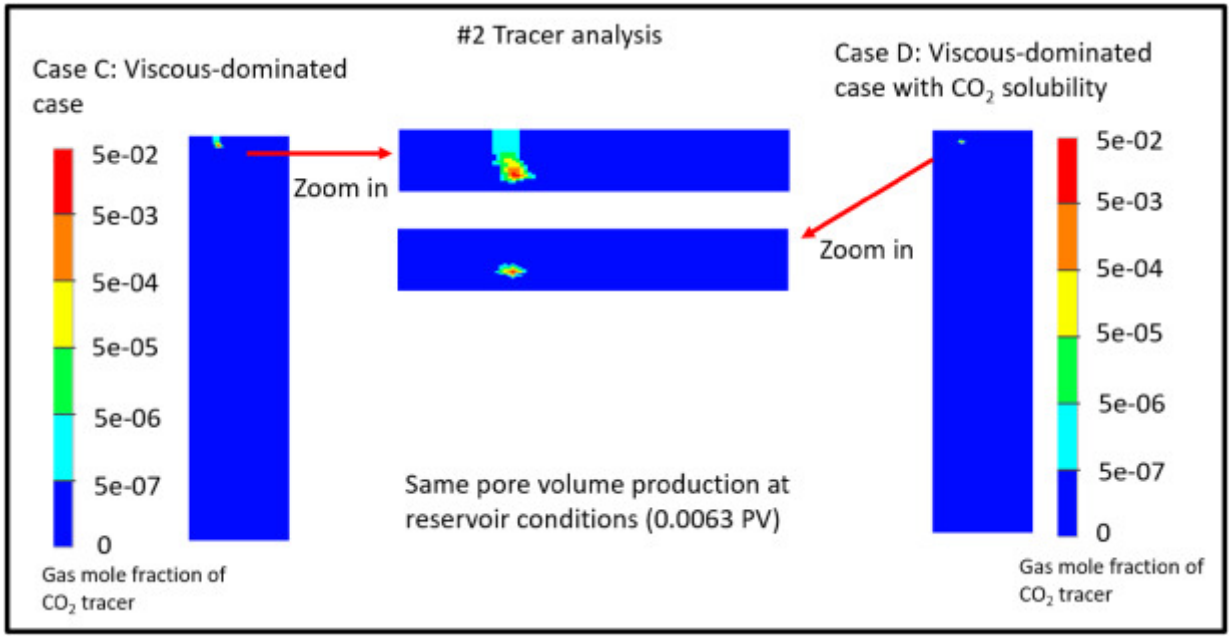

Download : Download high-res image (290KB) Download : Download full-size image

Fig. 8. Snapshots of tracer distribution in the viscous-dominated cases with (Case D on the right) and without CO_2 solubility (Case C on the left) at the end of tracer injection.

The question which now arises is: what is the mechanism by which CO_2 solubility in water acts to yield the results shown above? In other words, how does the CO_2 solubility in water delay the CO_2 production into the H_2 produced stream. Fig. 9 shows the CO_2 water mole fraction of representative cells in a ***preferential*** route and in a ***non-preferential*** route in the case with CO_2 solubility activated (Case B). The preferential routes are the areas where both H_2 and CO_2 can easily flow through during gas injection. The non-preferential routes mean that areas are

dominantly swept by CO_2 but mostly bypassed by H_2 during injection. The representative cell (Cell 1) of the ***non-preferential*** route is the same grid block as the one selected for the tracer analysis. The representative cell (Cell 2) of the ***preferential route*** is located to the left of Cell 1 and it has the same vertical position. The horizontal distance between of Cell 1 and Cell 2 is 1 m (10 grid blocks). We demonstrate the fluid behaviour during each stage of the operation below.

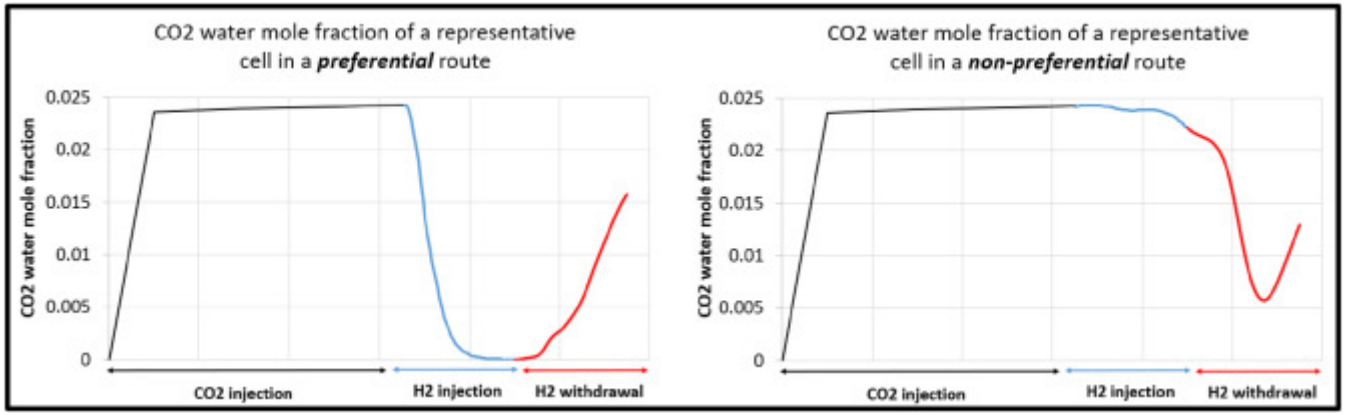

Download : Download high-res image (234KB) Download : Download full-size image

Fig. 9. CO_2 water mole fraction of representative cells: Cell 1 in a **preferential** route (left) and Cell 2 in a non-preferential route (right), respectively.

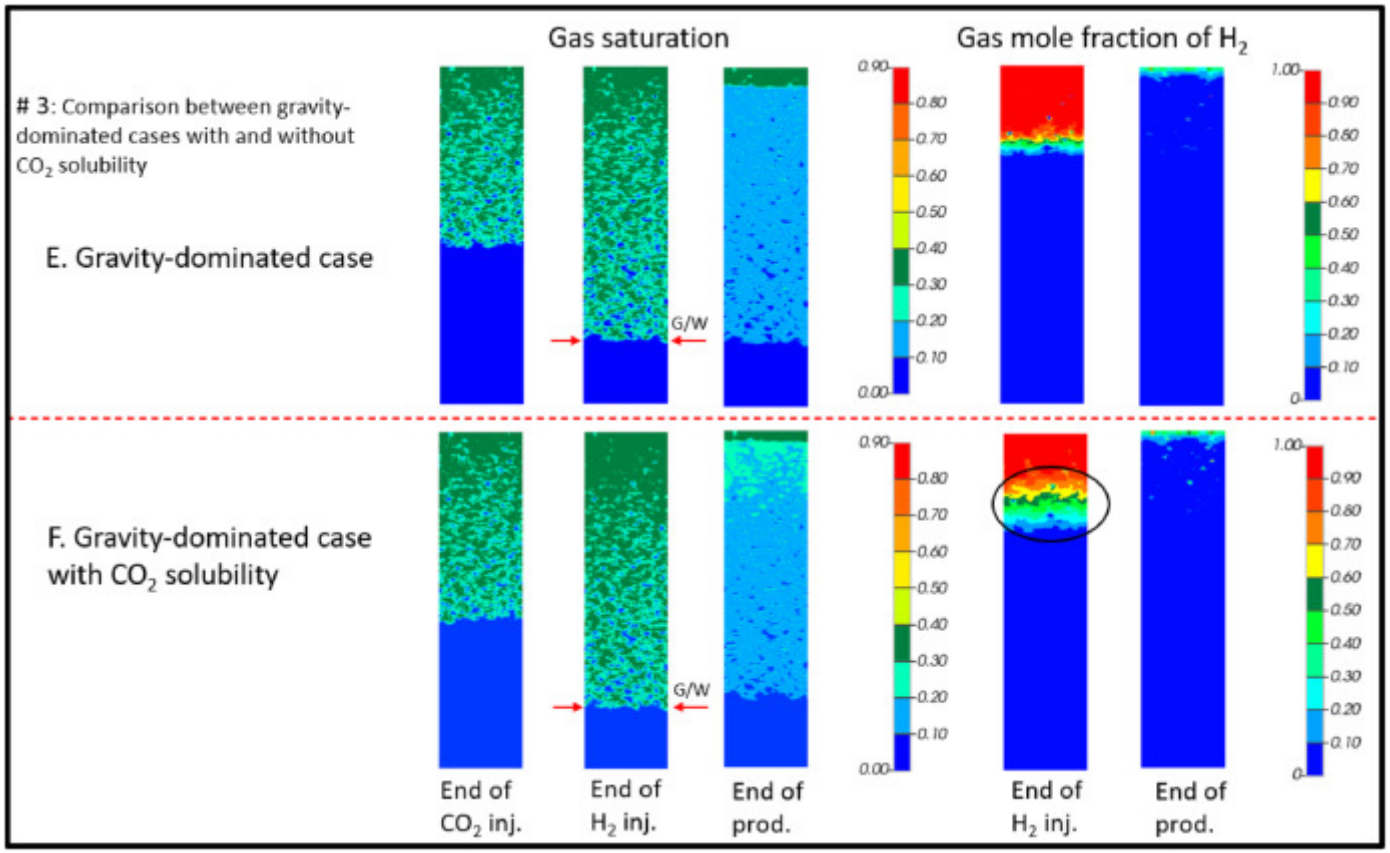

Download : Download high-res image (735KB) Download : Download full-size image

Fig. 10. Gas saturations and mole fractions of H_2 at the end of each cycle of the base model without CO_2 solubility (Case E at the top) and the case with CO_2 solubility (Case F at the bottom).

CO_2 injection

As seen in Fig. 9, CO_2 contacts and dissolves into the water during the CO_2 injection (black curves) until the equilibrium is reached (approximately 0.024 CO_2 mole fraction in water). This phenomenon occurs both in the representative cells of preferential and non-

preferential routes selected here. As mentioned above, the period of CO_2 injection is extended by 30% to compensate for its dissolution in water compared with the case without CO_2 solubility.

H_2 injection

When the working gas H_2 starts to be injected, CO_2 water mole fraction of the representative cell in the preferential route gradually decreases until no CO_2 is dissolved in the water (blue curves). This means that H_2 not only displaces the CO_2 in the gas phase but also vaporizes the dissolved CO_2. On the other hand, since H_2 hardly flows into the non-preferential routes, the gas phase in these bypassed areas is still predominantly consisting of CO_2. For this reason, the process of vaporization is very limited and therefore CO_2 water mole fraction does not decrease as much during the process of H_2 injection.

Back production

Unlike the process of H_2 injection, the flow during back production is a viscous-stable displacement process (since $\mu_{CO2}>\mu_{H2}$; $\mu_{water}>\mu_{CO2}$). Therefore, gas in both non-preferential routes and preferential routes starts to flow towards producers under the pressure gradient. When CO_2 solubility is not included, the CO_2 in the bypassed areas, especially those which are close to the producer, can flow into the preferential routes in neighbouring areas via viscous crossflow and then be produced. This leads to quick reduction in H_2 purity during the process of withdrawal. However, when CO_2 solubility is activated, the CO_2 contacts and redissolves into the water (now undersaturated with CO_2) in the preferential routes. In other words, CO_2 solubility enables the water surrounding the bypassed zone to act as a "filter" for CO_2. This explains the very limited distribution of CO_2 in gas phase shown in our tracer analysis. Since the CO_2-saturated water is still immobile, the CO_2 production is therefore delayed. Note that with increasing gas production, the upwards-flowing CO_2 gas can come out of solution and break through to the producer, but at a later time. Then, CO_2 starts to be produced and the H_2 purity level decreases (See Fig. 5).

Impacts of CO_2 solubility in gravity-dominated flow scenarios

In the previous section, we have demonstrated the impact of CO_2 solubility on the fluid behaviour and recovery performance (i.e., the level of H_2 purity) in the viscous-dominated flow regime. We now investigate the impacts of CO_2 solubility on the flow performance in the gravity-dominated scenario. This is referred to as the step #3 simulations described in Table 4.

As seen in Fig. 10, there is no evident infiltration or bypassing of H_2 in the gravity-dominated cases. Due to the density difference between H_2 and CO_2, H_2 is almost uniformly accumulated above the cushion gas of CO_2 in both Case E (CO_2 not soluble) and Case F (CO_2 soluble in water). However, the size of the mixing zone between CO_2 and H_2 is much expanded (as indicated by the black oval), when CO_2 solubility is

included. As mentioned above, H_2 not only displaces the CO_2 in the gas phase but also gradually strips the dissolved CO_2 out of the water. The extra amount of the vaporised CO_2 mixes with the injected H_2 and therefore a larger mixing zone is formed. As seen in Fig. 11, this has led to a slight reduction in the H_2 purity at the medium stage of the back production. Depending on the requirements for H_2 purity (90%–99.97%), such slight degradation in purity can lead to reductions in H_2 recovery by 3% and 6%, with a purity level above 99.97% and 98%, respectively. However, if the requirement of the purity level is reduced to 90%, the negative impacts of the CO_2 solubility is rather limited and the H_2 recovery is only lowered by approximately 1% in our cases (see Fig. 12).

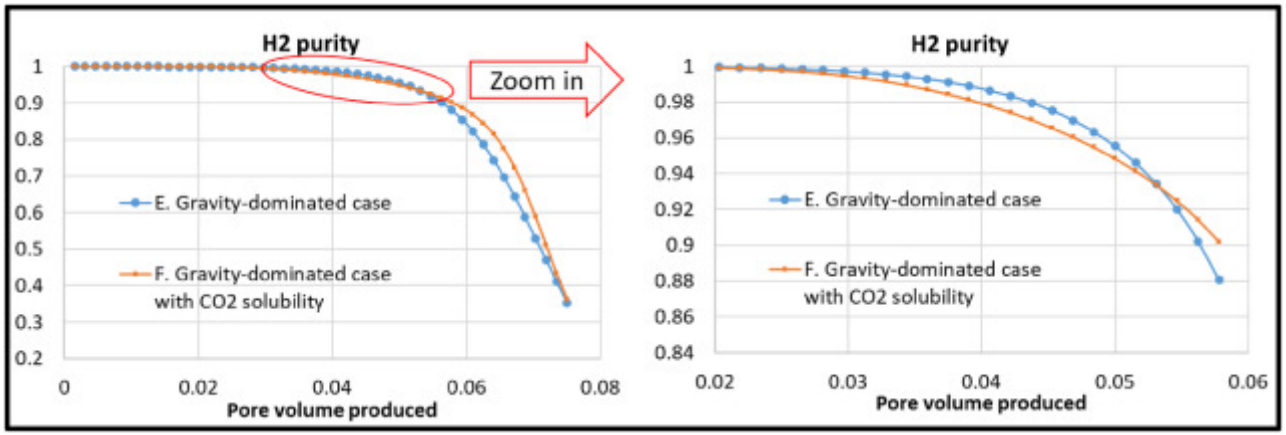

Download : Download high-res image (328KB) Download : Download full-size image

Fig. 11. The purity of back-produced H_2 of the gravity-dominated case (E) and the corresponding case with CO_2 solubility activated (F).

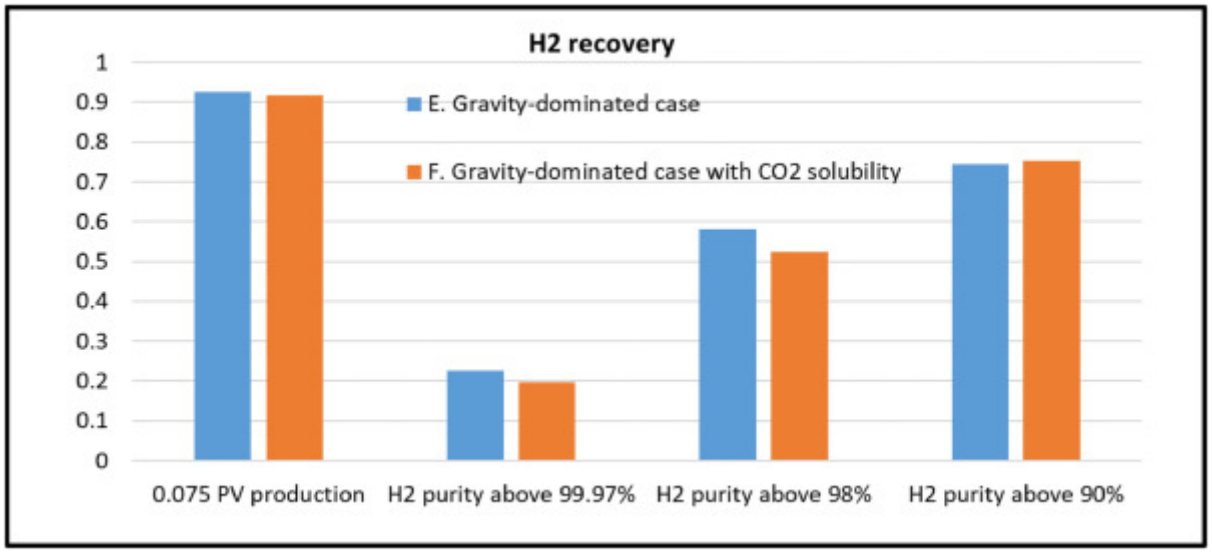

Fig. 12. Comparison of H_2 recovery between Case E&F at the end of 0.075 PV production, H_2 purity above 99.97%, 98% and 90%, respectively.

Very importantly, Fig. 13 is plotted to compare the recovery performance between the two end member scenarios, namely the viscous dominated and gravity dominated flow regimes. The two compared cases shown in Fig. 13 are both activated with the CO_2 solubility in water. It is found that the overall H_2 recovery performance is much better in the gravity-dominated scenarios than that in the viscous-dominated cases. Compared with the viscous-dominated case (Case B), an extra ***7%, 22%*** and ***27%*** H_2 recovery can be achieved in the gravity-dominated case (Case F), given the three threshold purity levels (99.97%, 98% and 90%).

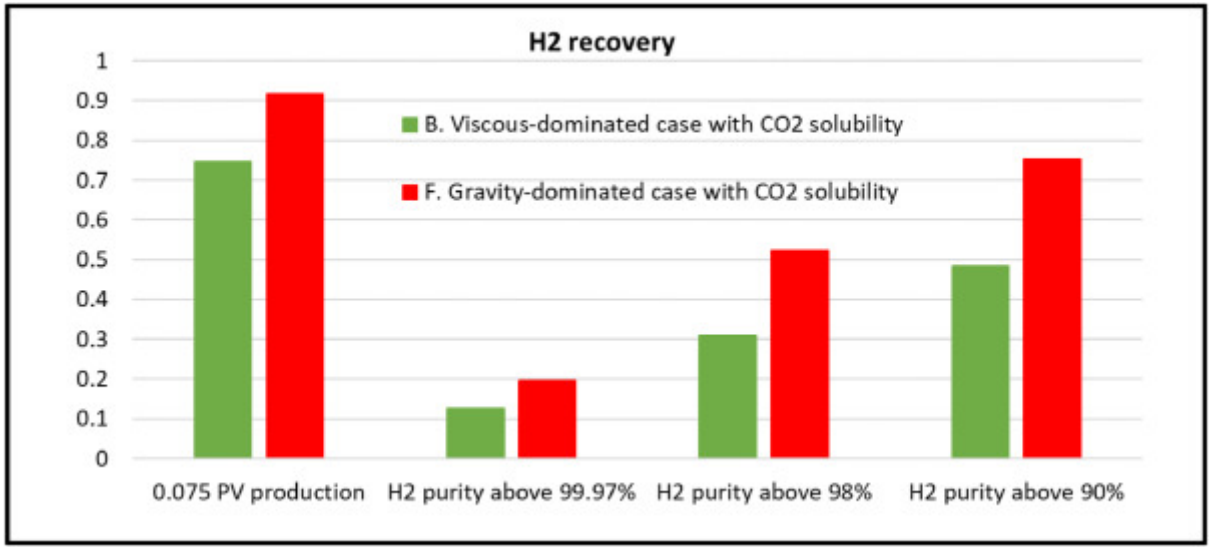

Download : Download high-res image (234KB) Download : Download full-size image

Fig. 13. Comparison of H_2 recovery between Case B&F at the end of 0.075 PV production, H_2 purity above 99.97%, 98% and 90%, respectively.

Conclusions

In our previous study [41], we have described and differentiated the role of various driving forces (viscous, gravity and capillary forces) during H_2 storage in subsurface porous media. Based on that work, we extend our research to analyse another important mechanism, viz., CO_2 solubility in water. With the use of very-fine scale full-compositional simulations ($\Delta x = 0.1$ m, in a 10 m × 80 m system), it is found that the CO_2 solubility can have either positive or negative impacts on the H_2 recovery performance, depending on the flow regime. Specifically, we have made the following four principal observations.

1. In cases with CO_2 solubility, the volume of CO_2 injected at reservoir conditions needs to be increased by approximately 30% in our system, to produce the same gas displacing front, as occurs in the case with no dissolution.

2.

In the viscous-dominated scenario, the issue of the dramatic reduction in H_2 purity is less severe, when CO_2 solubility is included. This is because the bypassed CO_2 will redissolve into water in neighbouring areas during back production, which retards the movement of CO_2 towards the producer, i.e., the so called "filter" effect for CO_2.

3. In the gravity-dominated scenario, the partitioning behaviour of CO_2 between gas and water has minor to moderate negative impacts on the H_2 recovery. H_2 not only displaces the CO_2 in gas phase but also gradually strips the dissolved CO_2 out of water. For this reason, the size of mixing zone of CO_2 and H_2 is enlarged, which leads to reductions in H_2 purity during back production.

4. The overall H_2 recovery performance is much better in the gravity-dominated scenarios than that in the viscous-dominated cases. This is because, in the viscous-dominated scenario H_2 may infiltrate and bypass the CO_2 and lead to early and dramatic reductions in H_2 purity during back production. Compared with the viscous-dominated case, an extra ***7%, 22%*** and ***27%*** H_2 recovery can be achieved in the gravity-dominated case, given the three important threshold purity levels (99.97%, 98% and 90%).

Declaration of competing interest

The authors declare that they have no known competing financial interests or personal relationships that could have appeared to influence the work reported in this paper.

Acknowledgements

Leverhulme Trust is thanked for supporting the Early-Career fellowship held by Dr. Gang Wang. Energi Simulation is thanked for funding the chair in CCUS and Reactive Flow Simulation at Heriot-Watt University held by Prof. Eric Mackay. Dr Gillian Pickup is part-funded by HyStorPor EPSRC EP/S027815/1. The authors would also like to appreciate the support by CMG for the use of CMG/GEM and Schlumberger for the use of Petrel.

List of abbreviations

C_a

Concentration of a species in the aqueous phase (mol/m^3)

f_{iw}

Fugacity of the component i in the aqueous phase

g

Gravitational acceleration constant

H

Reservoir thickness

H_i

Henry's Law constant

H_i^0

Reference Henry's Law constant

K_i

Permeability in directions i (i = x, y, z)

K_{rg}

Gas relative permeability

K_{rg}^{dr}

Gas relative permeability during drainage process

K_{rg}^{im}

Gas relative permeability during imbibition process

K_{rw}^{imb}

Imbibition relative permeability

K_{ro}

Oil relative permeability

K_{rw}

Water relative permeability

L

Reservoir length

P

Partial pressure in the gas phase under equilibrium conditions

P_c

Capillary pressure

P_i^0

Reference pressure

q

Flow rate

R

Gas constant

S_g

Gas saturation

S_{gc}

Critical gas saturation

S_{gr}

Trapped gas saturation (under the effect of gas trapping)

S_{gi}

Gas saturation at the start of the decreasing gas saturation process (under the effect of gas trapping)

S_{gmax}

Maximum attainable gas saturation

S_w

Water saturation

S_{wc}

Connate water saturation

T –

Temperature

u

- Flow velocity

V^{∞}

Partial molar volume of component i in the aqueous at infinite dilution

y_{iw}

Mole fraction of component i in aqueous phase

x, y, z

– Reservoir dimensions in x, y, and z directions

$\Delta x, \Delta y, \Delta z$

Cell size in x, y, and z directions

Δt

Time taken to inject a certain pore volume of fluid

$\Delta \rho$

Density difference between gas and water

$\emptyset$

- Porosity

σ_{gw}

- Interfacial tension between gas and water

μ_i

- Viscosity of phase i (i = g, w)

ρ_i

- Density of phase i (i = g, w)

θ

Contact angle between gas and water

PVI

Pore volume injected

Recommended articles

References

[1] IEA
Global energy & CO2 status report
Paris, France. Available at:
https://www.iea.org/reports/global-energy-co2-status-report-2019 (2019)
Google Scholar

[2] S. Fawzy, A.I. Osman, J. Doran, D.W. Rooney
Strategies for mitigation of climate change: a review
Environ Chem Lett, 18 (6) (2020), pp. 2069-2094
CrossRef View Record in Scopus Google Scholar

[3] C. Stark, M. Thompson, C.C. Committee
Net Zero the UK's contribution to stopping global warming
(2019)
Google Scholar

[4] IPCC
Global warming of 1.5°C
United Kingdom. Available at:
https://www.ipcc.ch/sr15/download/#full (2018)
Accessed: 06/02/2020
Google Scholar

[5] C.J. Quarton, S. Samsatli
Should we inject hydrogen into gas grids? Practicalities and whole-system value chain optimisation
Appl Energy, 275 (2020), Article 115172
Article Download PDF View Record in Scopus Google Scholar

[6] S. Samsatli, N.J. Samsatli
The role of renewable hydrogen and inter-seasonal storage in decarbonising heat – comprehensive optimisation of future renewable energy value chains
Appl Energy, 233–234 (2019), pp. 854-893
Article Download PDF View Record in Scopus Google Scholar

[7] R. Tarkowski
Underground hydrogen storage: characteristics and prospects
Renew Sustain Energy Rev, 105 (2019), pp. 86-94
Article Download PDF View Record in Scopus Google Scholar

[8] V. Reitenbach, L. Ganzer, D. Albrecht, B. Hagemann
Influence of added hydrogen on underground gas storage: a review of key issues
Environ Earth Sci, 73 (11) (2015), pp. 6927-6937

CrossRef View Record in Scopus Google Scholar

[9] A. Züttel, A. Remhof, A. Borgschulte, O. Friedrichs
Hydrogen: the future energy carrier
Phil Trans Math Phys Eng Sci, 368 (2010), pp. 3329-3342
CrossRef Google Scholar

[10] S. Schiebahn, T. Grube, M. Robinius, V. Tietze, B. Kumar, D. Stolten
Power to gas: technological overview, systems analysis and economic assessment for a case study in Germany
Int J Hydrogen Energy, 40 (12) (2015), pp. 4285-4294
Article Download PDF View Record in Scopus Google Scholar

[11] M. Ball, M. Wietschel
The future of hydrogen – opportunities and challenges
Int J Hydrogen Energy, 34 (2) (2009), pp. 615-627
Article Download PDF View Record in Scopus Google Scholar

[12] A. Midilli, I. Dincer
Hydrogen as a renewable and sustainable solution in reducing global fossil fuel consumption
Int J Hydrogen Energy, 33 (16) (2008), pp. 4209-4222
Article Download PDF View Record in Scopus Google Scholar

[13] M. Reuß, T. Grube, M. Robinius, P. Preuster, P. Wasserscheid, D. Stolten
Seasonal storage and alternative carriers: a flexible hydrogen supply chain model, vol. 200, Applied Energy (2017), pp. 290-302
Article Download PDF View Record in Scopus

[14] R.L. Wallace, Z. Cai, H. Zhang, K. Zhang, C. Guo
Utility-scale subsurface hydrogen storage: UK perspectives and technology
Int J Hydrogen Energy (2021)
Google Scholar

[15] D.J. Durbin, C. Malardier-Jugroot

Review of hydrogen storage techniques for on board vehicle applications
Int J Hydrogen Energy, 38 (34) (2013), pp. 14595-14617
Article Download PDF View Record in Scopus Google Scholar

[16] J. Mouli-Castillo, N. Heinemann, K. Edlmann
Mapping geological hydrogen storage capacity and regional heating demands: an applied UK case study
Appl Energy, 283 (2021), Article 116348
Article Download PDF View Record in Scopus Google Scholar

[17] Y. Qiu, S. Zhou, J. Wang, J. Chou, Y. Fang, G. Pan, W. Gu
Feasibility analysis of utilising underground hydrogen storage facilities in integrated energy system: case studies in China
Appl Energy, 269 (2020), Article 115140
Article Download PDF View Record in Scopus Google Scholar

[18] R. Ramachandran, R.K. Menon
An overview of industrial uses of hydrogen
Int J Hydrogen Energy, 23 (7) (1998), pp. 593-598
Article Download PDF View Record in Scopus Google Scholar

[19] D.G. Caglayan, N. Weber, H.U. Heinrichs, J. Linßen, M. Robinius, P.A. Kukla, D. Stolten
Technical potential of salt caverns for hydrogen storage in Europe
Int J Hydrogen Energy, 45 (11) (2020), pp. 6793-6805
Article Download PDF View Record in Scopus Google Scholar

[20] D.J. Evans, S. Holloway
A review of onshore UK salt deposits and their potential for underground gas storage
Geological Society, London, Special Publications, 313 (1) (2009), pp. 39-80
View Record in Scopus Google Scholar

[21] A.S. Lord, P.H. Kobos, D.J. Borns
Geologic storage of hydrogen: scaling up to meet city transportation demands

Int J Hydrogen Energy, 39 (28) (2014), pp. 15570-15582
Article Download PDF View Record in Scopus Google Scholar

[22] A. Ozarslan
Large-scale hydrogen energy storage in salt caverns
Int J Hydrogen Energy, 37 (19) (2012), pp. 14265-14277
Article Download PDF View Record in Scopus Google Scholar

[23] J. Scafidi, M. Wilkinson, S.M.V. Gilfillan, N. Heinemann, R.S. Haszeldine
A quantitative assessment of the hydrogen storage capacity of the UK continental shelf
Int J Hydrogen Energy, 46 (12) (2021), pp. 8629-8639
Article Download PDF View Record in Scopus Google Scholar

[24] H. Nazir, N. Muthuswamy, C. Louis, S. Jose, J. Prakash, M.E. Buan, C. Flox, S. Chavan, X. Shi, P. Kauranen, T. Kallio, G. Maia, K. Tammeveski, N. Lymperopoulos, E. Carcadea, E. Veziroglu, A. Iranzo, A.M. Kannan
Is the H2 economy realizable in the foreseeable future? Part II: H2 storage, transportation, and distribution
Int J Hydrogen Energy, 45 (41) (2020), pp. 20693-20708
Article Download PDF Google Scholar

[25] H. Blanco, A. Faaij
A review at the role of storage in energy systems with a focus on Power to Gas and long-term storage
Renew Sustain Energy Rev, 81 (2018), pp. 1049-1086
Article Download PDF View Record in Scopus Google Scholar

[26] R.A. Wattenbarger
Maximizing seasonal withdrawals from gas storage reservoirs
J Petrol Technol, 22 (1970), pp. 994-998
08
Google Scholar

[27] E. Escobar, G. Arteaga, A. Kemp

Underground natural gas storage in the UK: business feasibility case study
Proceedings of the SPE EUROPEC/EAGE Annual Conference and Exhibition (2011), 10.2118/143019-ms
Google Scholar

[28] M. Ball, M. Weeda
11 - the hydrogen economy—vision or reality?
M. Ball, A. Basile, T.N. Veziroğlu (Eds.), Compendium of hydrogen energy, Woodhead Publishing, Oxford (2016), pp. 237-266
Article Download PDF View Record in Scopus Google Scholar

[29] A.I. Osman, N. Mehta, A.M. Elgarahy, M. Hefny, A. Al-Hinai, A.a.H. Al-Muhtaseb, *et al.*
Hydrogen production, storage, utilisation and environmental impacts: a review
Environ Chem Lett, 20 (2022), pp. 153-188
CrossRef View Record in Scopus Google Scholar

[30] C.M. Oldenburg
Carbon dioxide as cushion gas for natural gas storage
Energy Fuels, 17 (1) (2003), pp. 240-246
View Record in Scopus Google Scholar

[31] K. Luboń, R. Tarkowski
Numerical simulation of hydrogen injection and withdrawal to and from a deep aquifer in NW Poland
Int J Hydrogen Energy, 45 (3) (2020), pp. 2068-2083
Article Download PDF View Record in Scopus Google Scholar

[32] M. Lysyy, M. Fernø, G. Ersland
Seasonal hydrogen storage in a depleted oil and gas field
Int J Hydrogen Energy, 46 (49) (2021), pp. 25160-25174
Article Download PDF View Record in Scopus Google Scholar

[33] W.T. Pfeiffer, S. Bauer
Subsurface porous media hydrogen storage – scenario development and simulation, vol. 76, Energy Procedia (2015), pp. 565-572

Article Download PDF View Record in Scopus

[34] F. Feldmann, B. Hagemann, L. Ganzer, M. Panfilov
Numerical simulation of hydrodynamic and gas mixing processes in underground hydrogen storages
Environ Earth Sci, 75 (16) (2016), p. 1165
View Record in Scopus Google Scholar

[35] J. Lewandowska-Śmierzchalska, R. Tarkowski, B. Uliasz-Misiak
Screening and ranking framework for underground hydrogen storage site selection in Poland
Int J Hydrogen Energy, 43 (9) (2018), pp. 4401-4414
Article Download PDF View Record in Scopus Google Scholar

[36] D. Zhou, F.J. Fayers, F.M. Orr Jr.
Scaling of multiphase flow in simple heterogeneous porous media
SPE Reservoir Eng, 12 (3) (1997), pp. 173-178
View Record in Scopus Google Scholar

[37] Y.-B. Chang, M. Lim, G. Pope, K. Sepehrnoori
CO2 flow patterns under multiphase flow: heterogeneous field-scale conditions
SPE Reservoir Eng, 9 (1994), pp. 208-216
03
View Record in Scopus Google Scholar

[38] D. Li, L.W. Lake
Scaling fluid flow through heterogeneous permeable media
(1995)
Google Scholar

[39] K. Sorbie, F. Feghi, G. Pickup, P. Ringrose, J. Jensen
Flow regimes in miscible displacements in heterogeneous correlated random fields
SPE Adv Technol, 2 (1994), pp. 78-87

02
Google Scholar

[40] A. Sainz-Garcia, E. Abarca, V. Rubi, F. Grandia
Assessment of feasible strategies for seasonal underground hydrogen storage in a saline aquifer
Int J Hydrogen Energy, 42 (26) (2017), pp. 16657-16666
Article Download PDF View Record in Scopus Google Scholar

[41] G. Wang, G. Pickup, K. Sorbie, E. Mackay
Scaling analysis of hydrogen flow with carbon dioxide cushion gas in subsurface heterogeneous porous media
Int J Hydrogen Energy (2021)
Google Scholar

[42] M. Akbarabadi, M. Piri
Relative permeability hysteresis and capillary trapping characteristics of supercritical CO2/brine systems: an experimental study at reservoir conditions
Adv Water Resour, 52 (2013), pp. 190-206
Article Download PDF View Record in Scopus Google Scholar

[43] S. Bachu, J.J. Adams
Sequestration of CO2 in geological media in response to climate change: capacity of deep saline aquifers to sequester CO2 in solution
Energy Convers Manag, 44 (20) (2003), pp. 3151-3175
Article Download PDF View Record in Scopus Google Scholar

[44] J. Bradshaw, S. Bachu, D. Bonijoly, R. Burruss, S. Holloway, N.P. Christensen, O.M. Mathiassen
CO2 storage capacity estimation: issues and development of standards
Int J Greenh Gas Control, 1 (1) (2007), pp. 62-68
Article Download PDF View Record in Scopus Google Scholar

[45] Cmg
CMG-GEM technical manual

Computer Modelling Group (2021)
Google Scholar

[46] D.-Y. Peng, D.B. Robinson
A new two-constant equation of state
Ind Eng Chem Fundam, 15 (1) (1976), pp. 59-64
CrossRef Google Scholar

[47] A. Danesh
PVT and phase behaviour of petroleum reservoir fluids (47)
Elsevier (1998)
Google Scholar

[48] Schlumberger
Petrel technical manual
Schlumberger Limited (2020)
Google Scholar

[49] B. Bennion, S. Bachu
Relative permeability characteristics for supercritical CO2 displacing water in a variety of potential sequestration zones
Proceedings of the SPE Annual Technical Conference and Exhibition (2005), 10.2118/95547-MS
Google Scholar

[50] F.M. Carlson
Simulation of relative permeability hysteresis to the nonwetting phase', SPE-10157-MS
Proceedings of the SPE annual technical conference and exhibition, Society of Petroleum Engineers, San Antonio, Texas (1981), pp. 4-7, 10.2118/10157-MS
October
View Record in Scopus Google Scholar

[51] C.S. Land

Comparison of calculated with experimental imbibition relative permeability
Soc Petrol Eng J, 11 (1971), pp. 419-425
04
Google Scholar

[52] A.H. Harvey
Semiempirical correlation for Henry's constants over large temperature ranges
AIChE J, 42 (5) (1996), pp. 1491-1494
View Record in Scopus Google Scholar

[53] Y.-K. Li, L.X. Nghiem
Phase equilibria of oil, gas and water/brine mixtures from a cubic equation of state and henry's law
Can J Chem Eng, 64 (3) (1986), pp. 486-496
CrossRef View Record in Scopus Google Scholar

[54] J.M. Smith, H.C. Van Ness, M.M. Abbott, M.T. Swihart
Introduction to chemical engineering thermodynamics
McGraw-Hill Education, United States of America (2017)
Google Scholar

[55] M. Lysyy, G. Ersland, M. Fernø
Pore-scale dynamics for underground porous media hydrogen storage
Adv Water Resour, 163 (2022), Article 104167
Article Download PDF View Record in Scopus Google Scholar

[56] R.A. Heidemann, J.M. Prausnitz
Equilibrium data for wet-air oxidation. Water content and thermodynamic properties of saturated combustion gases
Ind Eng Chem Process Des Dev, 16 (3) (1977), pp. 375-381
CrossRef Google Scholar

[57] R. Sander

Compilation of Henry's law constants, version 3.99
Atmos Chem Phys Discuss, 14 (21) (2014), pp. 29615-30521
CrossRef View Record in Scopus Google Scholar

[58] Z. Duan, R. Sun
An improved model calculating CO2 solubility in pure water and aqueous NaCl solutions from 273 to 533 K and from 0 to 2000 bar
Chem Geol, 193 (3) (2003), pp. 257-271
Article Download PDF View Record in Scopus Google Scholar

[59] E.M. Thaysen, S. McMahon, G.J. Strobel, I.B. Butler, B.T. Ngwenya, N. Heinemann, M. Wilkinson, A. Hassanpouryouzband, C.I. McDermott, K. Edlmann
Estimating microbial growth and hydrogen consumption in hydrogen storage in porous media
Renew Sustain Energy Rev, 151 (2021), Article 111481
Article Download PDF View Record in Scopus Google Scholar

[60] G. Wang, G. Pickup, K. Sorbie, E. Mackay, A. Skauge
Numerical study of CO2 injection and the role of viscous crossflow in near-miscible CO2-WAG
J Nat Gas Sci Eng, 74 (2020), Article 103112
Article Download PDF View Record in Scopus Google Scholar

[61] G. Wang, G.E. Pickup, K.S. Sorbie, E.J. Mackay
Analysis of compositional effects on global flow regimes in CO2 near-miscible displacements in heterogeneous systems
Transport Porous Media, 129 (3) (2019), pp. 743-759
CrossRef View Record in Scopus Google Scholar

[62] K. Liu, C. Song, V. Subramani
Hydrogen and syngas production and purification technologies
John Wiley & Sons (2010)
Google Scholar

Cited by (0)